

## Autoimmune Target in Heymann Nephritis Is a Glycoprotein with Homology to the LDL Receptor

RAKTIMA RAYCHOWDHURY, JOHN L. NILES, ROBERT T. MCCLUSKEY, JOHN A. SMITH\*

The pathogenesis of Heymann nephritis, a rat model of human membranous glomerulonephritis, depends on the interaction of autoantibodies with a renal glycoprotein (GP330) on glomerular podocytes. Partial complementary DNAs coding for GP330 were isolated and sequenced. The deduced amino acid sequence from 4.3 kilobases of complementary DNA contains the sequences identical to two peptides derived from the isolated glycoprotein. The deduced amino acid sequence of this protein contains regions with homology to the human low density lipoprotein (LDL) receptor, an indication that GP330 and the LDL receptor may be members of the same gene family. Autoantibodies from the kidneys of rats with Heymann nephritis reacted with a nonglycosylated segment of GP330 that contains cysteine-rich 40–amino acid repeats, which are also features of the LDL receptor. GP330 is also similar in some regions to the mouse epidermal growth factor precursor.

**G**LYCOPROTEIN GP330, SO DESIGNATED because it has a molecular size of 330 kD, was identified by Kerjaschki and Farquhar (1) as the pathogenic autoantigen in Heymann nephritis. Heymann nephritis is a rat model of human membranous glomerulonephritis (2), a chronic renal disease usually manifested by the nephrotic syndrome and in some cases by progressive renal failure. The rat glycoprotein is found on the apical plasmalemmal domain of some epithelial cells, in particular glomerular podocytes, proximal renal tubules, intestine, lung (type II pneumocytes), epididymis, and yolk sac (3). The analogous human protein has been identified (4) that reacts with antibodies eluted from the glomeruli of some specimens of membranous glomerulonephritis (5). Although the biological function of GP330 is unknown, its presence on absorptive epithelial cells and the finding that it is normally concentrated in coated pits suggest that it may be a receptor, as has been demonstrated for the LDL receptor (6) and other receptors (7). There is evidence that a 76-kD serum protein may be a ligand for GP330 (8).

We purified the GP330 protein from a crude renal tubule-rich fraction of normal

Lewis rat kidneys by immunoaffinity chromatography (9). The purified protein showed a single band of 440 kD on SDS-polyacrylamide gel electrophoresis (SDS-PAGE). In our experiments the protein designated GP330 consistently appeared at a higher molecular size. The purified protein was digested with trypsin, the peptides were isolated by reversed-phase high-performance liquid chromatography (HPLC), and the sequences of several peptides were determined by automated Edman degradation (10). The sequence of one peptide, L-Y-W-V-D-A-F-F-D, was used to design a synthetic oligonucleotide, [TAC<sup>T</sup>-TGG-GT(I)-GAC<sup>T</sup>-GC(I)-TT<sup>T</sup>-TT<sup>T</sup>-GA].

Five putative, partial GP330 cDNA clones were identified by screening a rat kidney  $\lambda$ gt11 expression library (Clontech) with a specific polyclonal rabbit antiserum to rat GP330 (9, 11). Inserts of 0.4 kb, 0.6

kb, 1.4 kb, and two of 2.4 kb were subcloned into Bluescript (Stratagene) and sequenced (12). To determine whether the deduced partial sequences of GP330 are similar to sequences of other protein, we used the FASTP program in a computer-based search of the National Biomedical Research Foundation protein database (13). Protein sequence similarities were found among rat GP330, the human LDL receptor (6), and the mouse epidermal growth factor (EGF) precursor (14). The oligonucleotide probe hybridized to the 5' end of the 1.4-kb insert (Fig. 1, asterisk). The oligonucleotide-hybridizing region contained the coding sequence defined by the tryptic peptide, which is partially identical to the LDL receptor (Fig. 2, region A). The DNA sequence of the 0.4-kb insert is contained within the 0.6-kb insert, which is contained within the 1.4-kb insert. Two overlapping 2.4-kb inserts provided an additional 2.9-kb nucleotide sequence. The protein sequence deduced from the 2.9-kb DNA sequence contained a sequence identical to that of another tryptic peptide, V-L-V-V-N-P-W-L-T-Q-V (Fig. 1, two asterisks), a 29–amino acid transmembrane segment (Fig. 1), and a 188–amino acid cytoplasmic tail. The LDL receptor and GP330 are similar in six separate regions (Fig. 2, regions A to F). Both GP330 and the LDL receptor contain cysteine-rich ligand-binding repeat sequences (~40–amino acid residues per repeat) in regions D and E (Fig. 2). At least 13 consensus repeats are distributed within the GP330 molecule in regions D and E (Fig. 1), whereas the LDL receptor has seven ligand-binding repeats at its NH<sub>2</sub>-terminus (6) (Fig. 1, crosshatched). We used another computer program, BESTFIT (15), to determine the percent similarity of GP330 protein with LDL receptor. The 1.4-kb region contains 478 amino acids, and this region is 41% homologous to the LDL receptor, whereas the percent similarity in the 2.9-kb region (884 amino acids) is 35%. Because the LDL receptor and GP330 are

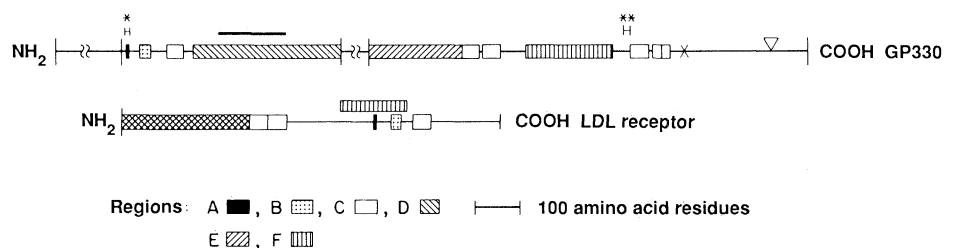


**Fig. 1.** Comparison of the structure of GP330 deduced from the nucleotide sequence of five partial cDNAs and the LDL receptor (6). The GP330 protein sequences of the two regions between the break marks have not been determined. The location of two GP330 tryptic peptide sequences are indicated by segments marked with one or two asterisks. The protein sequence deduced from the 2.9-kb DNA sequence contained a 29–amino acid transmembrane segment (marked X) and the 188–amino acid cytoplasmic tail (stop codon marked as open triangle). Regions A to F correspond to the amino acid sequences shown in Fig. 2.

R. Raychowdhury and J. A. Smith, Departments of Molecular Biology and Pathology, Massachusetts General Hospital, Boston, MA 02114.  
J. L. Niles, Departments of Medicine and Pathology, Massachusetts General Hospital, Boston, MA 02114.  
R. T. McCluskey, Department of Pathology, Massachusetts General Hospital, Boston, MA 02114.

\*To whom correspondence should be addressed.

similar to one another, they may be members of the same gene family. The  $\alpha$  and  $\beta$  chains of the human complement proteins C8 and the C9 precursor each contain a single copy of the LDL receptor ligand-binding repeat (16). GP330 also contains cysteine-rich EGF precursor repeats (Figs. 1 and 2, region C), which are different from the LDL receptor ligand-binding repeat. The 1.4-kb insert contains only one repeat (Fig. 2, top line of region C), whereas three full and two half repeats are distributed in the 2.9-kb region (Figs. 1 and 2, region C). Furthermore, GP330, the LDL receptor, and EGF precursor display protein-sequence similarities in nonrepetitive regions (Figs. 1 and 2, regions A, B, and F). Homology to the LDL receptor and EGF precursor has also been observed in a 500-kD liver protein, so-called LDL receptor-related protein (LRP) (17). The cytoplasmic tail of GP330 contains three homologous repeats of seven amino acids (IFENPMY,

NVENQNY, and NIENPIY), whereas LRP contains two repeats (EIGNPTY and NFTNPVY), and the LDL receptor has one (NFDNPVY). This signal is crucial for endocytosis of the LDL receptor (6).

We also found that GP330- $\beta$ -galactosidase fusion proteins (18) containing polypeptides coded for by the 0.4-, 0.6-, and 1.4-kb inserts reacted strongly with autoantibodies eluted from the kidneys of rats with Heymann nephritis (19). Thus, each fusion protein contains at least one antigenic site recognized by the pathogenic autoantibodies. The polypeptide derived from the 0.4-kb insert (Fig. 1, solid bar above region D) contains three and one half LDL receptor ligand-binding repeats, although region D contains eight repeats. Further, since this region of GP330 is NH<sub>2</sub>-terminal to the transmembrane segment, it is likely that this antigenic site is displayed in a region of GP330 extending from the external surface of an epithelial cell membrane. Whether

additional immunoreactive regions are present in the regions flanking this site remains unclear. Additional fusion proteins derived from the two overlapping, 2.4-kb inserts did not react with the autoantibodies, although each of these fusion proteins contains additional LDL receptor ligand-binding repeats (Figs. 1 and 2, region E). Since the fusion proteins are not glycosylated, the antigenic sites must be on the protein component of GP330.

It is believed that in Heymann nephritis the interaction of autoantibodies with GP330 on glomerular podocytes leads to formation of immune complexes that are shed into the adjacent basement membrane, where they aggregate to form insoluble deposits. Evidence of shedding of GP330 complexes from glomerular epithelial cells has also been obtained *in vitro* with cultured cells (20). Why some GP330-containing complexes are shed rather than being efficiently internalized by receptor-mediated

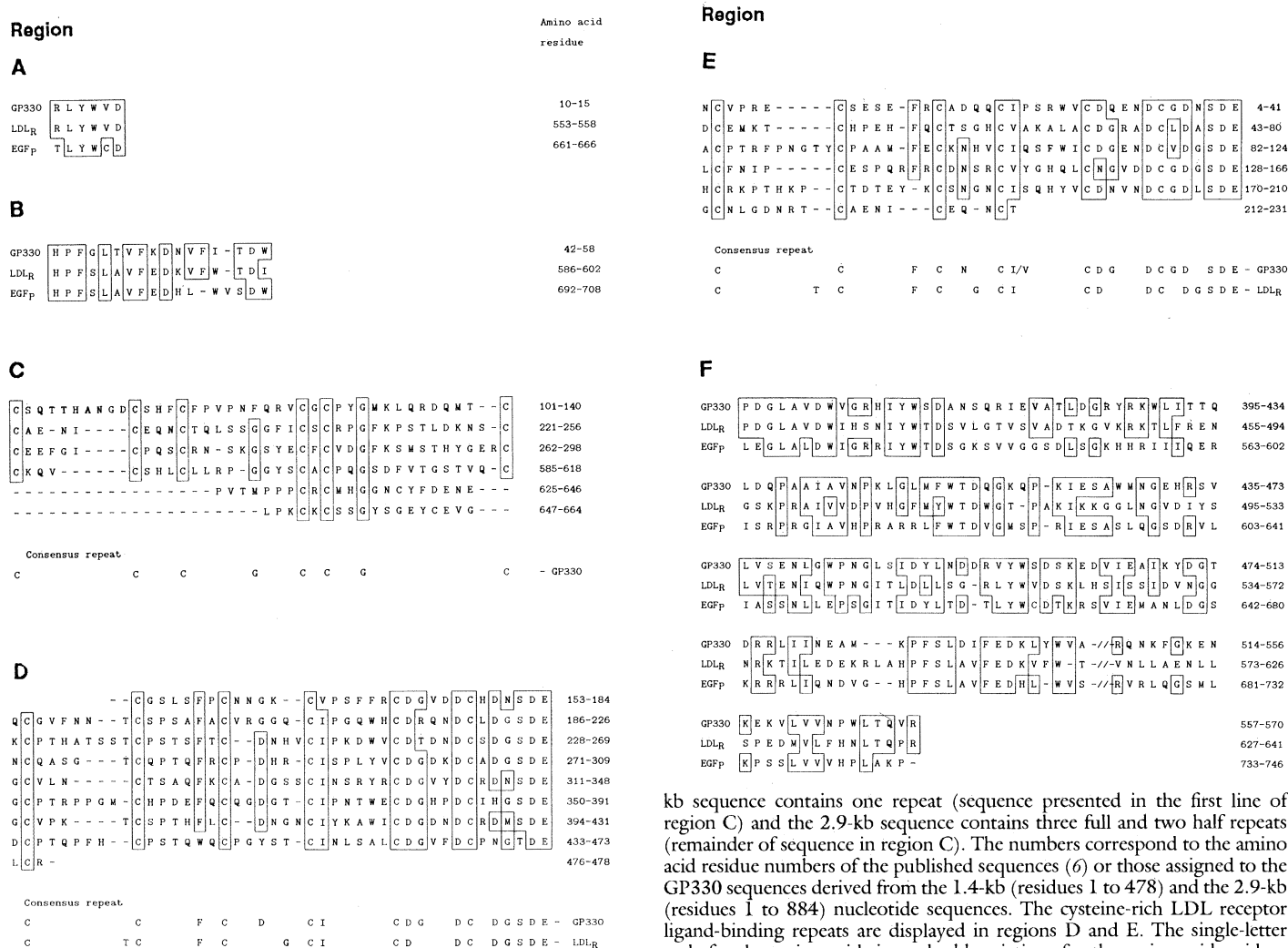


**Fig. 2.** Amino acid sequence comparisons of GP330, LDL receptor, and EGF precursor. GP330, the LDL receptor, and EGF precursor display sequence homology in nonrepetitive regions as shown by regions A, B, and F. The cysteine-rich EGF precursor repeats are shown in region C. The 1.4-

kb sequence contains one repeat (sequence presented in the first line of region C) and the 2.9-kb sequence contains three full and two half repeats (remainder of sequence in region C). The numbers correspond to the amino acid residue numbers of the published sequences (6) or those assigned to the GP330 sequences derived from the 1.4-kb (residues 1 to 478) and the 2.9-kb (residues 1 to 884) nucleotide sequences. The cysteine-rich LDL receptor ligand-binding repeats are displayed in regions D and E. The single-letter code for the amino acids is used; abbreviations for the amino acid residues are A, Ala; C, Cys; D, Asp; E, Glu; F, Phe; G, Gly; H, His; I, Ile; K, Lys; L, Leu; M, Met; N, Asn; P, Pro; Q, Gln; R, Arg; S, Ser; T, Thr; V, Val; W, Trp; and Y, Tyr. The gaps were inserted to optimize the alignment. LDLR, LDL receptor; EGFp, EGF precursor.

endocytosis, as would be expected of a receptor in coated pits, is unknown. How much of the GP330 molecule is shed in the form of immune complexes is also unknown. The eventual availability of a full-length cDNA should allow a detailed analysis of how much of this protein is shed rather than endocytosed and why. An analysis of the antigenic sites recognized by the pathogenic autoantibodies by use of nested sets of synthetic peptides (21) and a determination of their location in this membrane glycoprotein may reveal the autoimmune basis of Heymann nephritis and its human counterpart.

#### REFERENCES AND NOTES

1. D. Kerjaschki and M. G. Farquhar, *Proc. Natl. Acad. Sci. U.S.A.* **79**, 5557 (1982).
2. W. Heymann, D. B. Hackle, S. Harwood, J. L. P. Hunter, *Proc. Soc. Exp. Biol. Med.* **100**, 660 (1959); D. Kerjaschki and M. G. Farquhar, *J. Exp. Med.* **157**, 667 (1983).
3. S. Doxsey, D. Kerjaschki, M. G. Farquhar, *J. Cell Biol.* **97**, 178a (1983); F. Chatelet *et al.*, *Am. J. Pathol.* **122**, 512 (1986).
4. D. Kerjaschki *et al.*, *Am. J. Pathol.* **129**, 183 (1987).
5. J. L. Niles *et al.*, *Kidney Int.* **31**, 338 (1987).
6. T. Yamamoto *et al.*, *Cell* **39**, 27 (1984); J. L. Goldstein *et al.*, *Annu. Rev. Cell Biol.* **1**, 1 (1985).
7. A. Ullrich *et al.*, *Nature* **309**, 418 (1984); A. McClelland, L. C. Kuhn, F. H. Ruddle, *Cell* **39**, 267 (1984); C. Schneider, M. J. Owen, D. Banville, J. G. Williams, *Nature* **311**, 675 (1984); K. Drickamer, J. F. Mamon, G. Binns, J. O. Leung, *J. Biol. Chem.* **259**, 770 (1984); K. E. Mostov, M. Friedlander, G. Blobel, *Nature* **308**, 37 (1984).
8. J. J. Kanalas and S. P. Makker, *J. Immunol.* **141**, 4152 (1988).
9. J. Gutmann *et al.*, *Am. J. Physiol.* in press.
10. W. W. Wong, L. B. Klickstein, J. A. Smith, J. H. Weis, D. T. Fearon, *Proc. Natl. Acad. Sci. U.S.A.* **82**, 7711 (1985).
11. T. V. Huynh, R. A. Young, R. W. Davis, in *DNA Cloning: A Practical Approach*, D. M. Glover, Ed. (IRL Press, Oxford, 1985), vol. 1, pp. 49–78.
12. F. Sanger and A. R. Coulson, *J. Mol. Biol.* **94**, 441 (1975).
13. D. J. Lipman and W. R. Pearson, *Science* **227**, 1435 (1985).
14. A. Gray, T. J. Dull, A. Ullrich, *Nature* **303**, 722 (1983); J. Scott *et al.*, *Science* **221**, 236 (1983).
15. J. Devereux, P. Haeberli, O. Smithies, *Nucleic Acids Res.* **12**, 387 (1984).
16. A. G. Rao *et al.*, *Biochemistry* **26**, 3556 (1987); O. M. Z. Howard, A. G. Rao, J. M. Sodez, *ibid.*, p. 3565; K. K. Stanley *et al.*, *EMBO J.* **4**, 375 (1985).
17. J. Herz *et al.*, *EMBO J.* **7**, 4119 (1988).
18. D. M. Bai *et al.*, *J. Biol. Chem.* **261**, 12395 (1986).
19. K. Kamata, L. G. Baird, M. E. Erikson, A. B. Collins, R. T. McCluskey, *J. Immunol.* **135**, 2400 (1985).
20. G. Camussi *et al.*, *ibid.*, p. 2409.
21. R. A. Houghton, *Proc. Natl. Acad. Sci. U.S.A.* **82**, 5231 (1985).
22. This work was supported by a grant from Hoechst Aktiengesellschaft (Frankfurt/Main, West Germany) and NIH grants P01-DK38452 and R01-DK18729. The authors acknowledge L.-W. Lin and L. B. Klickstein for technical discussions. We also thank M. Foucre, P. Gallant, and G. Hannigan for technical assistance.

6 January 1989; accepted 21 April 1989

## Neptune Cloud Structure at Visible Wavelengths

H. B. HAMMEL

Digital images of Neptune showing cloud structure at visible wavelengths were obtained in July 1988. A discrete bright feature was detected both at 6190 Å (a weak methane absorption band in the visible) and at 8900 Å (a stronger methane band in the near infrared). The images also revealed that Neptune's southern pole was bright relative to planetary mid-latitudes at 6190 Å but not 8900 Å. The implications of these findings for atmospheric rotation and structure are discussed. The detection of discrete features at visible wavelengths is of special importance to the upcoming Voyager encounter with Neptune: the wide-angle camera has a 6190 Å filter similar to that used for these observations.

FOR THE PAST DECADE, THE PLANET Neptune has shown a remarkable amount of variability on time scales ranging from hours to years (1). In 1987, the diurnal variation of Neptune's disk-integrated flux was caused by a single atmospheric inhomogeneity (discrete feature), with the observed fluctuations attributable to the appearance and disappearance of this feature during planetary rotation (2). Many earlier images of the planet show discrete cloud features on Neptune, but these images were always obtained at 8900 Å, a strong

near-infrared methane absorption band where the contrast between features and the surrounding atmosphere is enhanced (3–5). No images at visible wavelengths have shown discrete features (5), even though their presence at these wavelengths was inferred from disk-integrated photometry that showed strong diurnal variation (6, 7). In this paper I present new images obtained at visible wavelengths that show discrete cloud features.

The new images of Neptune (shown in Fig. 1) are a subset of data obtained with the University of Hawaii 2.24-m telescope (Mauna Kea Observatory, Hawaii) on 11 to

15 July 1988 through filters centered on three methane bands (6190, 7270, and 8900 Å) and three nearby continuum regions (6340, 7490, and 8260 Å). Each pixel of the 576 by 385 charge-coupled device (CCD) array corresponded to 0.202 arc sec on the sky. The disk of Neptune subtended approximately 2.3 arc sec; the size of the seeing disk was about 0.5 arc sec. The images were reduced by subtracting a constant bias level (typically on the order of 5340 data numbers), and then dividing by a flat-field frame. I obtained flat-field frames by exposing the CCD to the illuminated inner surface of the telescope dome through each filter each night. The final flat field for each night at each wavelength was the average of all flats obtained at that wavelength that night, normalized to unity.

Figure 1 shows a time sequence of Neptune images at two methane band wavelengths. At both wavelengths, a discrete bright feature can be seen moving from left to right as the planet rotates. The images on the left (at 6190 Å) show discrete cloud structure; all earlier images showing discrete features were obtained at 8900 Å (shown in the right-hand column). Each image in Fig. 1 is expanded from the original by a factor of 4 by means of a sinc interpolation function. In practice, this technique smooths across pixel boundaries. Only large-scale features are true features associated with Neptune (see Fig. 1); "features" that are smaller than a tenth of a planetary diameter are not true features on the planet, but pixel-to-pixel variations in the detector.

From the feature's apparent motion as the planet rotates, an atmospheric rotation period can be derived. In the past, a number of different rotation periods were deduced from the variability of Neptune, ranging from  $17.0 \pm 0.05$  up to  $18.4 \pm 0.01$  hours (4). Because the diverse measurements of Neptune's period came from observations at a variety of wavelengths ranging from the visible (6190 Å) out to the near infrared (at 1.25 and 2.2 μm), the discrepancy of periods was attributed to wavelength, that is, different wavelengths were probing to different depths in the atmosphere (6, 8, 9). In 1988, the dominant atmospheric rotation period was  $17.7 \pm 0.5$  hours, based on observations of transits of the brightest feature in several series of 8900 Å images (10) and on disk-integrated photometry of the planet at 8900 Å (11). But the 17.0-hour period found in 1986 and 1987 was also determined at 8900 Å (2). Furthermore, measurements of the feature's location on the disk of the planet indicate that in 1988 the same feature was detected at both 6190 and 8900 Å (Fig. 1). Thus the period at 6190 Å is the same as that found from 8900

Jet Propulsion Laboratory, Pasadena, CA 91109.